Math Geosci (2010) 42: 49–64
DOI 10.1007/s11004-009-9257-x

Measurement of Areas on a Sphere Using Fibonacci and Latitude–Longitude Lattices

Álvaro González

Received: 3 June 2009 / Accepted: 16 November 2009 / Published online: 28 November 2009

Abstract The area of a spherical region can be easily measured by considering which sampling points of a lattice are located inside or outside the region. This point-counting technique is frequently used for measuring the Earth coverage of satellite constellations, employing a latitude–longitude lattice. This paper analyzes the numerical errors of such measurements, and shows that they could be greatly reduced if the Fibonacci lattice were used instead. The latter is a mathematical idealization of natural patterns with optimal packing, where the area represented by each point is almost identical. Using the Fibonacci lattice would reduce the root mean squared error by at least 40%. If, as is commonly the case, around a million lattice points are used, the maximum error would be an order of magnitude smaller.

Keywords Spherical grid · Golden ratio · Equal-angle grid · Non-standard grid · Fibonacci grid · Phyllotaxis

1 Introduction

The area of a region is easy to measure, without explicitly considering its boundaries, by determining which points of a lattice are inside or outside the region. This point-counting method is commonly applied to estimating areas on a plane (Bardsley 1983; Jarái et al. 1997; Howarth 1998; Gundersen et al. 1999; Baddeley and Jensen 2004). A related issue is how to approximate the region boundaries from this sampling (Barclay and Galton 2008). Point-counting on the sphere is commonly used for estimating the Earth coverage of satellite constellations (Kantsiper and Weiss 1998; Feng et al. 2006), the fraction of the Earth's surface efficiently seen by one or more

Á. González (✉)
Departamento de Ciencias de la Tierra, Universidad de Zaragoza, C. Pedro Cerbuna, 12, 50009 Zaragoza, Spain
e-mail: Alvaro.Gonzalez@unizar.es

satellites. In the simplest case, each satellite covers a circular region (cap), so the constellation covers a complex set of isolated and/or overlapping caps (Kantsiper and Weiss 1998). Similarly, some maps designed for global earthquake forecasting depict earthquake-prone regions as complex sets of up to tens of thousands of caps (Kossobokov and Shebalin 2003; Kafka 2007; González 2009). To assess these forecasts it is necessary to measure the fraction of the Earth's area covered by these regions (Kafka 2007). Analytical solutions exist if the spherical region has a known, regular or polygonal shape (Kimerling 1984; Bevis and Cambareri 1987; Sjöberg 2006). The area of a set of caps on the sphere has a complex analytical solution (Kantsiper and Weiss 1998), which unfortunately does not indicate whether any particular location on the surface of the sphere is covered.

The numerical error of point counting should ideally decrease rapidly as the lattice density increases. Numerous works deal with errors on the plane (Bardsley 1983, Jarái et al. 1997; Howarth 1998; Gundersen et al. 1999; Baddeley and Jensen 2004). Some particular cases using latitude–longitude lattices were analyzed elsewhere (Kantsiper and Weiss 1998). In automated counting, the computation time is directly proportional to the number of lattice points. Satellite constellation coverage (Ochieng et al. 2002) or the areas marked on rapidly-updated earthquake forecasting maps (González 2009) need continuous monitoring, implying a trade-off between accuracy and computational load. Thus it is important to find lattices able to measure areas as efficiently as possible. On the plane, the regular hexagonal lattice provides optimal sampling (Conway and Sloane 1998). On the sphere, it is impossible to arrange regularly more than 20 points (the vertices of a dodecahedron), and the optimum configuration of a large number of points is problem-specific (Saff and Kuijlaars 1997; Conway and Sloane 1998; Williamson 2007; Gregory et al. 2008). For optimal point-counting, the area represented by every point should be almost the same.

Traditionally, the latitude–longitude lattice is used for measuring Earth coverage (Kantsiper and Weiss 1998; Ochieng et al. 2002; Feng et al. 2006). However, it is very inhomogeneous (Fig. 1), requiring non-uniform weighting of the point contributions. Also, its number of points is restricted by geometrical constraints. The Fibonacci lattice is a particularly appealing alternative (Dixon 1987, 1989, 1992; Fowler et al. 1992; Svergun 1994; Kozin et al. 1997; Swinbank and Purser 1999, 2006a, 2006b; Winfield and Harris 2001; Nye 2003; Hannay and Nye 2004; Purser and Swinbank 2006; Purser 2008). Being easy to construct, it can have any odd number of points (Swinbank and Purser 2006b), and these are evenly distributed (Fig. 1) with each point representing almost the same area. For the numerical integration of continuous functions on a sphere, it has distinct advantages over other lattices (Hannay and Nye 2004; Purser and Swinbank 2006). This paper demonstrates that for measuring the areas of spherical caps, the Fibonacci lattice is much more efficient than its latitude–longitude counterpart. After describing both lattices (Sects. 2 and 3), it is explained how to use them for measuring cap areas (Sect. 4) and how the error of this measurement is assessed (Sect. 5). The error results obtained from an extensive Monte Carlo simulation are described, and to some extent explained analytically (Sect. 6). The conclusions are set out in the final section.

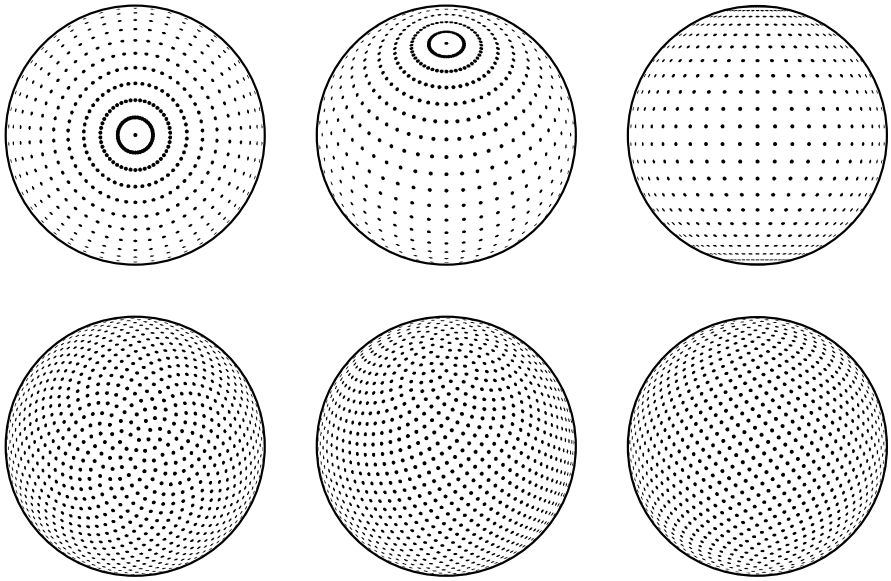

Fig. 1 Latitude–longitude lattice (*top*) and Fibonacci lattice (*bottom*), with 1014 and 1001 points, respectively. Orthographic projections, centered at the pole (*left*), latitude 45° (*middle*), and equator (*right*). In the Fibonacci lattice, the points are much more evenly spaced, and the axial anisotropy is much smaller

2 Latitude–Longitude Lattice

The latitude–longitude lattice is the set of points located at the intersections of a grid of meridians and parallels, separated by equal angles of latitude and longitude (Fig. 1). This is the latitude–longitude grid (Swinbank and Purser 2006b; Williamson 2007) or equal-angle grid (Gregory et al. 2008). The points concentrate towards the poles, due to the converging meridians, resulting in high anisotropy.

The number of points, P, depends on the angular spacing, δ, between grid lines. Since $\delta = 180°/k$ with $k = 1, 2, \ldots,$

$$P = 2k(k-1) + 2. \tag{1}$$

That is the number of meridians ($2k$) times the number of parallels ($k-1$), plus the two poles. Frequently, to evaluate satellite coverage (Feng et al. 2006), $\delta = 0.25°$, so more than a million points are used.

3 Fibonacci Lattice

The points of the Fibonacci lattice are arranged along a tightly wound generative spiral, with each point fitted into the largest gap between the previous points (Fig. 2). This spiral is not apparent (Fig. 1) because consecutive points are spaced far apart from each other. The most apparent spirals join the points closest to each other, and form crisscrossing sets (Swinbank and Purser 2006b). The points are evenly spaced

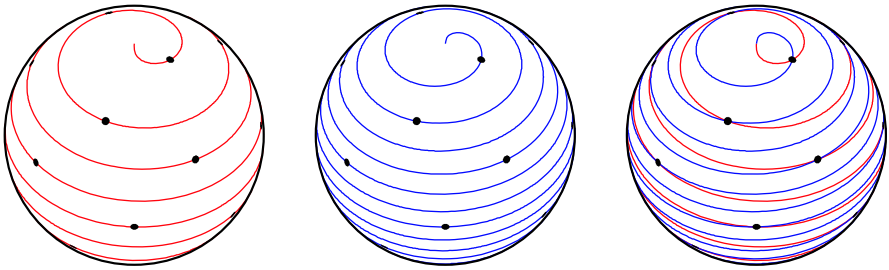

Fig. 2 Generative spirals of a Fibonacci lattice with 21 points. The angle turn between consecutive points along a spiral is based on the golden ratio (Φ): either the golden angle, $360°\Phi^{-2} \simeq 137.5°$ (first spiral, *red*), or its complementary, $360°\Phi^{-1} \simeq 222.5°$ (second spiral, *blue*). No point is placed at the poles. Orthographic projection, centered at longitude 0°, latitude 45°

in a very isotropous way. The next subsections describe how to construct the lattice used in this paper, and the history of the Fibonacci lattice in various research fields.

3.1 Lattice Construction

The Fibonacci lattice is named after the Fibonacci ratio. The Fibonacci sequence was discovered in ancient India (Singh 1985; Knuth 1997) and rediscovered in the middle ages by Leonardo Pisano, better known by his nickname Fibonacci (Sigler 2002). Each term of the sequence, from the third onwards, is the sum of the previous two: $0, 1, 1, 2, 3, 5, 8, 13, 21, \ldots$. Given two consecutive terms, F_i and F_{i+1}, a Fibonacci ratio is F_i/F_{i+1}. As first proved by Robert Simson in 1753, this quotient, as $i \to \infty$, quickly approaches the golden ratio, defined as $\Phi = 1 + \Phi^{-1} = (1+\sqrt{5})/2 \simeq 1.618$. The Fibonacci lattice differs from other spiral lattices on the sphere (Weiller 1966; Klíma et al. 1981; Rakhmanov et al. 1994; Saff and Kuijlaars 1997; Chukkapalli et al. 1999; Bauer 2000; Hüttig and Stemmer 2008) in that the longitudinal turn between consecutive points along the generative spiral is the golden angle, $360°(1 - \Phi^{-1}) = 360°\Phi^{-2} \simeq 137.5°$, or its complementary, $360°\Phi^{-1} \simeq 222.5°$. Some lattice versions replace Φ by its rational approximant, a Fibonacci ratio.

The golden angle optimizes the packing efficiency of elements in spiral lattices (Ridley 1982, 1986). This is because the golden ratio is the most irrational number (Weisstein 2002), so periodicities or near-periodicities in the spiral arrangement are avoided, and clumping of the lattice points never occurs (Ridley 1982; Dixon 1987; Prusinkiewicz and Lindenmayer 1990; Jean 1994; Hannay and Nye 2004; Purser and Swinbank 2006). The lattice version used here (Swinbank and Purser 2006b) is probably the most homogeneous one. It is generated with a Fermat spiral (also known as the cyclotron spiral) (Vogel 1979; Dixon 1987, 1992), which embraces an equal area per equal angle turn, so the area between consecutive sampling points, measured along the spiral, is always the same (Swinbank and Purser 2006b). Also, its first and last points are offset from the poles, leading to a more homogeneous polar arrangement (Purser and Swinbank 2006; Swinbank and Purser 2006b) than in other versions (Svergun 1994; Kozin et al. 1997; Nye 2003; Hannay and Nye 2004; Purser and Swinbank 2006). When a Fibonacci ratio is used (Svergun 1994; Kozin

et al. 1997; Nye 2003; Hannay and Nye 2004), the number of lattice points is $F+1$, where $F>1$ is a term of the Fibonacci sequence. The lattice used here is instead based on the golden ratio and can have any odd number of points. To elaborate the lattice (Swinbank and Purser 2006b), let N be any natural number. Let the integer i range from $-N$ to $+N$. The number of points is

$$P = 2N + 1, \tag{2}$$

and the spherical coordinates, in radians, of the ith point are

$$\mathrm{lat}_i = \arcsin\left(\frac{2i}{2N+1}\right), \tag{3}$$

$$\mathrm{lon}_i = 2\pi i \Phi^{-1}. \tag{4}$$

This pseudocode provides the geographical coordinates in degrees

For $i = -N, (-N+1), \ldots, (N-1), N$, Do {
$\mathrm{lat}_i = \arcsin(\frac{2i}{2N+1}) \times 180°/\pi$
$\mathrm{lon}_i = \mathrm{mod}(i, \Phi) \times 360°/\Phi$
If $\mathrm{lon}_i < -180°$, then $\mathrm{lon}_i = 360° + \mathrm{lon}_i$
If $\mathrm{lon}_i > 180°$, then $\mathrm{lon}_i = \mathrm{lon}_i - 360°$
} End Do

Here, arcsin returns a value in radians, while $\mathrm{mod}(x, y)$ returns the remainder when x is divided by y, removing the extra turns of the generative spiral. For example, $\mathrm{mod}(6, \Phi) = 6 - 3 \times \Phi$. The last two lines keep the longitude range from $-180°$ to $+180°$. Every point of this lattice is located at a different latitude, providing a more efficient sampling than the latitude–longitude lattice. The middle point, $i = 0$, is placed at the equator ($\mathrm{lat}_0 = 0$ and $\mathrm{lon}_0 = 0$). Each of the other points $(\mathrm{lat}_i, \mathrm{lon}_i)$ with $i \neq 0$, has a centrosymmetric one with $(-\mathrm{lat}_i, -\mathrm{lon}_i)$. The lattice as a whole is not centrosymmetric.

The longitudinal turn between consecutive lattice points along the spiral (4) is the complementary of the golden angle (Swinbank and Purser 1999, 2006b). To use the golden angle instead, we can substitute (4) by

$$\mathrm{lon}_i = -2\pi i \Phi^{-2}. \tag{5}$$

With (4), the spiral progresses eastwards, while the minus sign of (5) indicates a westward progression. A remark not found elsewhere is that the lattice points are placed at the intersections between these Fermat spirals of opposite chirality, except at the poles (Fig. 2). For drawing the spirals, i is made continuous in (3), (4), and (5), and ranges from $(-N - 1/2)$ to $(N + 1/2)$. The $1/2$ term accounts for the polar offset (Purser and Swinbank 2006; Swinbank and Purser 2006b).

3.2 Lattice History

The Fibonacci lattice is a mathematical idealization of patterns of repeated plant elements, such as rose petals, pineapple scales, or sunflower seeds (Fig. 3). The study of

Fig. 3 Spherical Fibonacci lattices in Nature: an oblique view of two *Mammillaria solisioides*. The elements of many plants form Fibonacci lattices, for example, the areoles (spine-bearing nodes) of *Mammillaria* cacti (Fowler et al. 1992; Kuhlemeier 2007)

these arrangements is known as Phyllotaxis (Prusinkiewicz and Lindenmayer 1990; Jean 1994; Adler et al. 1997; Kuhlemeier 2007). The Bravais brothers (Bravais and Bravais 1837) were the first to describe them using a spiral lattice on a cylinder. They argued that the most common angle turn between consecutive elements along this spiral in plants is the golden angle. The latter provides optimum packing (Ridley 1982, 1986), maximizing the exposure to light, rain and insects for pollination (Maciá 2006). Structures in cells and viruses also follow this pattern (Erikson 1973). In some experiments, elements are spontaneously ordered on roughly hemispherical Fibonacci lattices because the system tends to minimize the strain energy (Li et al. 2005) or to avoid periodic organization (Douady and Couder 1992). Unwrapping the cylindrical Fibonacci lattice produces a flat one (Bravais and Bravais 1837; Hannay and Nye 2004; Swinbank and Purser 2006b), frequently used for numerical integration (Zaremba 1966; Niederreiter 1992; Niederreiter and Sloan 1994; Sloan and Joe 1994).

Projecting the cylindrical Fibonacci lattice to the sphere generates the spherical version (Hannay and Nye 2004; Swinbank and Purser 2006b). This can be generalized to arbitrary surfaces of revolution (Ridley 1986; Dixon 1992). The first graphs of spherical Fibonacci lattices used, as here, the golden ratio and a Fermat spiral (Dixon 1987, 1989, 1992). A version based on the Fibonacci ratio is used in the modeling of complex molecules (Vriend 1990; Svergun 1994; Kozin et al. 1997). In this case (Svergun 1994; Kozin et al. 1997), a "+" sign in the formula for the longitude should be substituted by "×" (D. Svergun, personal communication, 2009). Versions with the golden ratio serve to simulate plants realistically (Fowler et al. 1992) and to design golf balls (Winfield and Harris 2001). The latter method was used by Douglas C. Winfield (B. Moore and D. C. Winfield, personal communication, 2009) in the Starshine-3 satellite (Fig. 4). The spherical Fibonacci lattice is a highly efficient sampling scheme for integrating continuous functions (Nye 2003; Hannay and Nye 2004; Purser and Swinbank 2006), as was observed in magnetic resonance imaging (Ahmad et al. 2007). It is also advantageous

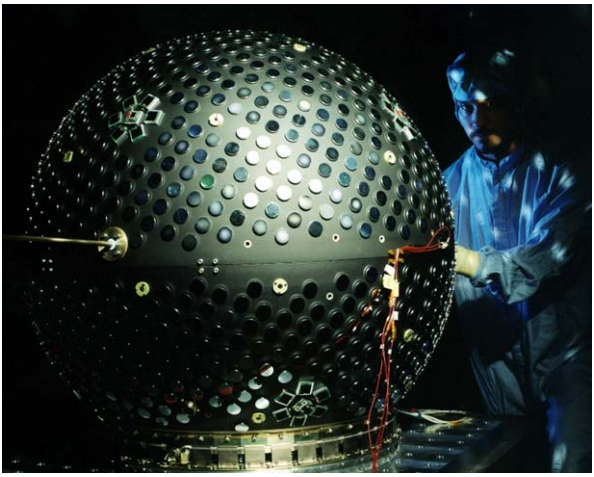

Fig. 4 The Starshine-3 satellite (Maley et al. 2002; Lean et al. 2006) had 1500 mirrors arranged on a spherical Fibonacci lattice. Picture by Michael A. Savell and Gayle R. Fullerton, taken while the satellite was being inspected by John Vasquez. Reproduced by courtesy of the US Naval Research Laboratory

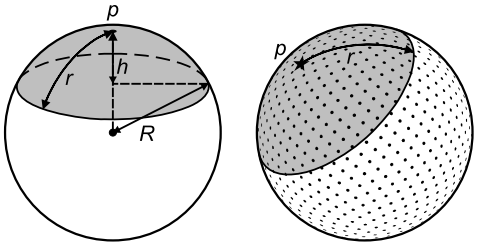

Fig. 5 Measurement of cap area. The cap (*left*), centered at p, has height h and great-circle radius r, and is a region of a sphere with radius R. Placed at random (*right*), its area can be estimated by considering the lattice points it covers

for providing grid nodes in global meteorological models (Michalakes et al. 1999; Swinbank and Purser 1999, 2006a, 2006b; Purser and Swinbank 2006; Purser 2008).

4 Area Measurement

The area measurement starts by finding which points of the lattice are inside the considered region. This is expressed by a Boolean function f_i, such that $f_i = 1$ if the ith point is inside, and $f_i = 0$ otherwise (Kantsiper and Weiss 1998). If the region is a cap with radius r, it suffices to measure d, the shortest distance (great-circle distance) between the sampling point and the cap center (Fig. 5)

$$f_i = \begin{cases} 1 & \text{if } d \le r, \\ 0 & \text{if } d > r. \end{cases} \tag{6}$$

Each lattice point must be assigned a weight, w_i, proportional to the area it represents. Then the estimate, $\widetilde{A}$, of the region area A, is measured considering the sphere area, A_S, and summing the contribution of all P points of the lattice

$$A \simeq \widetilde{A} = \frac{A_S \sum_{i=1}^{P} f_i w_i}{\sum_{i=1}^{P} w_i}. \tag{7}$$

The weights depend on the lattice type, as described below.

4.1 Weights in the Latitude–Longitude Lattice

The weights should be inversely proportional to the point density, which here increases towards the poles (Fig. 1). The linear spacing between parallels is constant. The length of a parallel is $2\pi R\cos(\text{lat})$, where R is the sphere radius. In any parallel, there is the same number of lattice points ($2k$), so their density is inversely proportional to (Kantsiper and Weiss 1998; Van den Dool 2007)

$$w_i = \cos(\text{lat}_i). \tag{8}$$

4.2 Weights in the Fibonacci Lattice

Thanks to the even distribution of points in this lattice, the same weight can be assumed for all of them (Purser and Swinbank 2006; Swinbank and Purser 2006b), namely

$$w_i = 1. \tag{9}$$

Each point represents the area corresponding to its Voronoi cell (Thiessen polygon). This is the region of positions closer to the corresponding lattice point than to any other (Evans and Jones 1987; Na et al. 2002). Using the exact area of each Voronoi cell as weight for its lattice point (Ahmad et al. 2007) would improve the area measurement only slightly. The average cell area equals A_S/P. Here, regardless of P, only the areas of less than ten cells, located at the polar regions, differ by more than $\sim$2% from this value (Swinbank and Purser 2006b). As P increases, proportionally fewer cells depart significantly from the average area. Unlike the latitude–longitude lattice, the homogeneity of the Fibonacci lattice improves with the number of points.

5 Error Assessment

This section details how to assess the error involved in measuring the area of spherical caps placed at random on the sphere. A good way to measure the homogeneity of a spherical lattice is to compare the proportion of lattice points in spherical regions with the normalized areas of the regions (Cui and Freeden 1997). For this task, it is natural to use spherical caps (Saff and Kuijlaars 1997; Damelin and Grabner 2003; Brauchart 2004), which moreover appear in the applications mentioned in the introduction. The area of a spherical cap (see Fig. 5) is

$$A_C = 2\pi Rh = 2\pi R^2\left(1 - \cos\frac{r}{R}\right). \tag{10}$$

The normalized cap area is

$$F = \frac{A_C}{A_S} = \frac{1 - \cos(r/R)}{2}, \tag{11}$$

where $A_S = 4\pi R^2$ is the sphere area. The absolute error of measuring a single cap is the difference between the estimated fraction and the actual one

$$E = \left|\widetilde{A}_C/A_S - F\right|. \tag{12}$$

This depends on the lattice type, the number of points, and the size and location of the cap. If $E = 0$, the cap gets its fair share of weighted lattice points. If $A_C = 0$, $E = 0$. For any cap, E is the same as for the complementary cap $A'_C = 1 - A_C$, so it suffices to consider caps not larger than a hemisphere ($A_C = A_S/2$).

The error is characterized here numerically using a Monte Carlo method. In each particular realization, a cap is randomly placed. Every point of the sphere has the same probability of becoming the cap center, p, with coordinates

$$\text{lat}_p = \frac{180^\circ}{\pi} \arcsin(2X - 1), \tag{13}$$

$$\text{lon}_p = 360^\circ X - 180^\circ. \tag{14}$$

Here X is a random number, chosen with uniform probability in the range $[0, 1]$, independently for each equation. The area of this jth cap is estimated, and its corresponding error is E_j. The process is repeated for a total of n independently located caps of the same size, providing a sample of n values of E. The root mean squared error is (Weisstein 2002)

$$\text{rmse} = \sqrt{\frac{1}{n}\sum_{j=1}^{n} E_j^2}. \tag{15}$$

The supremum error in (12) for caps of any size, for a given lattice type and P, using $w_i = 1$, is the spherical cap discrepancy (Saff and Kuijlaars 1997; Damelin and Grabner 2003; Brauchart 2004). It cannot be determined exactly with a Monte Carlo simulation because it might result from a cap size not used, or a location not sampled. However, it is unfortunately difficult to compute explicitly (Damelin and Grabner 2003). The maximum E measured for the Fibonacci lattice is a lower bound to its spherical cap discrepancy.

6 Results

This section details the maximum errors and root mean squared errors measured with the Monte Carlo simulation detailed in the previous section. Thirteen lattice configurations of each type, from $P \simeq 10^2$ to $P \simeq 10^6$, were analyzed. The chosen values of P increase in logarithmic steps, as accurately as possible ($P \simeq 10^2, 10^{7/3}, 10^{8/3}, 10^3, \ldots$). It is impossible to use identical P for both lattices because P is odd in the Fibonacci lattice, but even in the latitude–longitude lattice. Moreover, there are considerably fewer possible values of P in the latter. For each configuration, 200 different cap sizes were used, from $A_C = 0.0025A_S$ to $A_C = 0.5A_S$ in steps of $0.0025A_S$. To obtain smooth results, $n = 60,000$ was chosen for each cap size and lattice configuration. In total, 312 million caps were measured (2 lattice types × 13

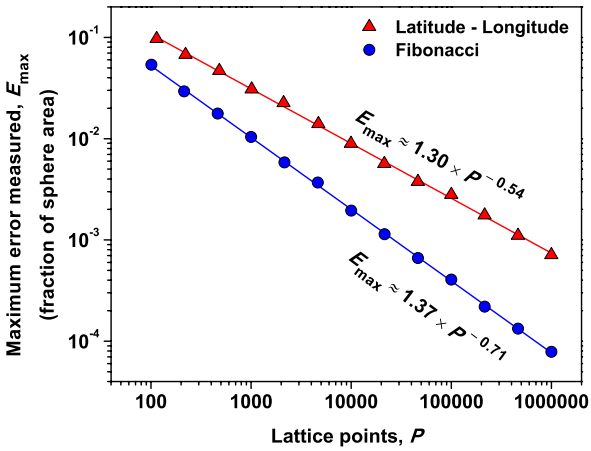

Fig. 6 Maximum error measured for randomly located spherical caps of any size. For area measurements on the Earth, about a million points are frequently used (Feng et al. 2006), for which the maximum error would be an order of magnitude smaller in the Fibonacci lattice

values of $P \times 200$ cap sizes $\times 60{,}000$ caps). After optimization, the calculation took 43 days of CPU time using 2.8 GHz, 64-bit processors.

The maximum E measured, for caps of any size and location, is represented in Fig. 6. For the Fibonacci lattice, it is much lower and decays faster than for the latitude–longitude lattice, despite the non-uniform weighting of points of the latter.

The rmse depends on the lattice type, number of points and cap size, as shown in Fig. 7. Because of the symmetry of the latitude–longitude lattice, any hemispherical cap covers one half of the points of the lattice, and (thanks to the point weighs) the estimation is perfect ($E = 0$ and rmse $= 0$). This exception aside, rmse tends to increase with the cap area, in a non-trivial way, which is more complex for the latitude–longitude lattice than for the Fibonacci lattice.

Figure 8 (top) shows the maximum values of rmse of each curve. They follow parallel power laws

$$\text{rmse}_{\text{max}} \simeq k P^{-3/4}, \tag{16}$$

with $k \simeq 0.505$ for the latitude–longitude lattice, and $k \simeq 0.362$ for the Fibonacci lattice. Interpolating for the same P, the rmse_{max} would be $0.505/0.362 \simeq 40\%$ larger in the latitude–longitude lattice.

6.1 Analytical Approach to the Root Mean Squared Error

The scaling shown in Fig. 8 can be explained using arguments from similar problems in the plane (Kendall 1948; Huxley 1987, 2003). The number of points of a regular square lattice enclosed by a sufficiently smooth, closed curve placed at random can be expressed as (Huxley 2003)

$$P_{\text{in}} = AM^2 + D, \tag{17}$$

where A is the area enclosed by the curve, M is the inverse to the lattice spacing, and D is the discrepancy. The nominal spacing of a spherical lattice is $\sqrt{A_S/P}$ (Swinbank

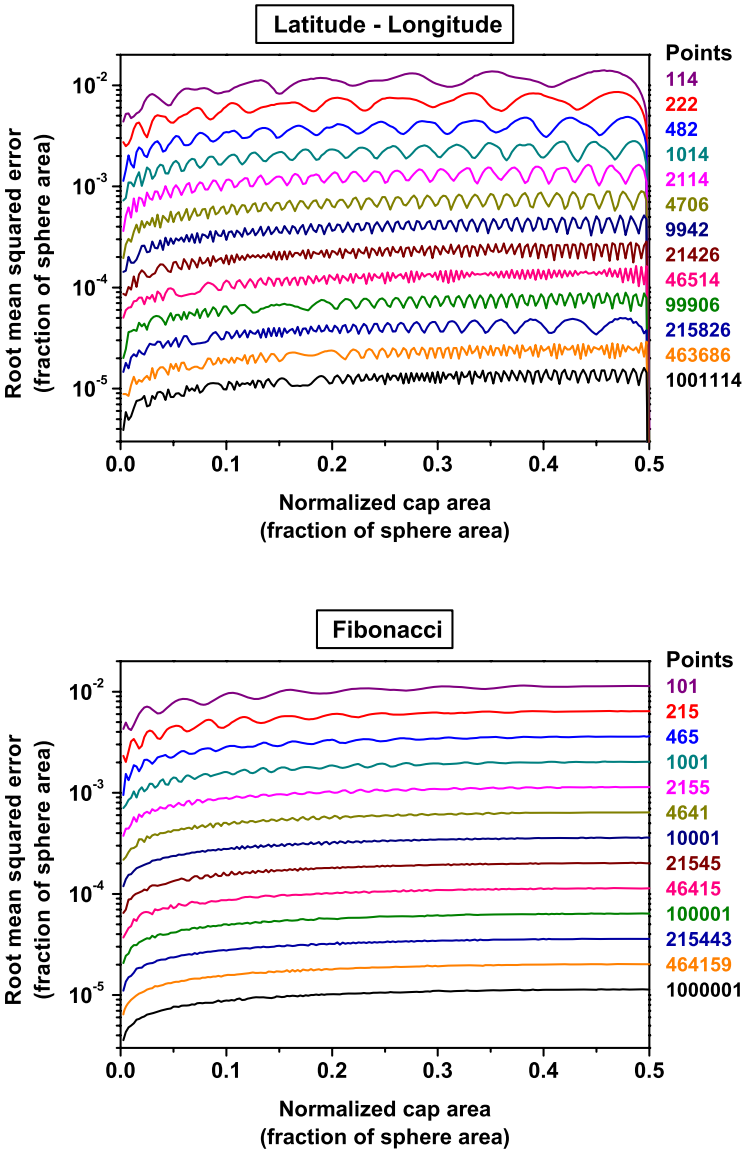

Fig. 7 Root mean squared error. For randomly placed caps which occupy an area fraction given by the abscissas, the *curve* indicates the root mean squared error of the area measurement. Each curve corresponds to a different number of lattice points, labeled at its right. For similar lattice densities, the Fibonacci lattice provides smaller and more homogeneous errors

and Purser 2006b). Assuming that the Fibonacci lattice is regular enough,

$$M \approx \sqrt{\frac{P}{A_S}}. \tag{18}$$

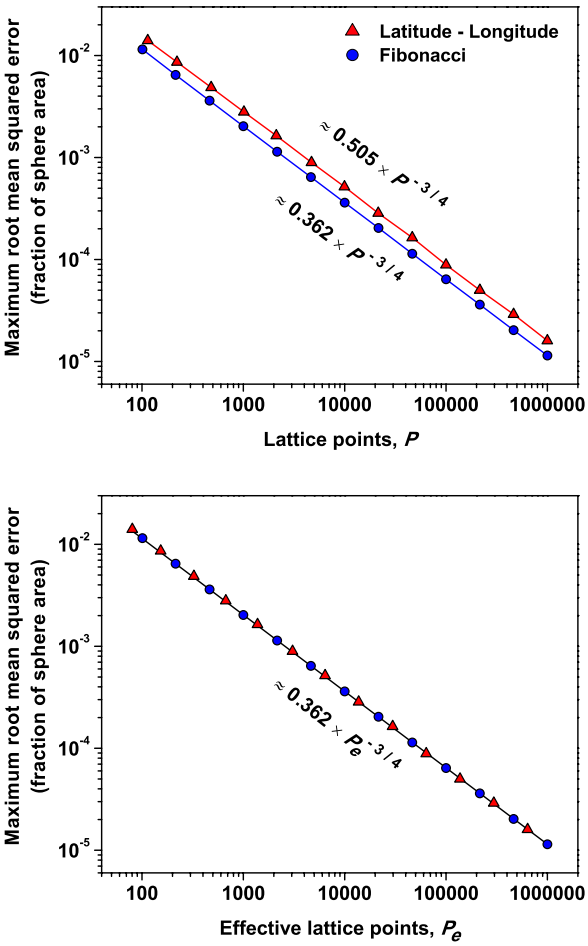

Fig. 8 Scaling of the maximum root mean squared error. Each *dot* corresponds to the maximum value of a curve in Fig. 7. (*Top*) For the same number of points, the values would be about 40% smaller for the Fibonacci lattice. (*Bottom*) The latitude–longitude lattice is inefficient because the effective (weighted) number of points is smaller than the real one. Considering this fact, the results collapse to a single function. The power-law decay and its exponent agree with analytical scaling arguments (see text)

Substituting this into (17),

$$P_{\text{in}} \approx P\frac{A}{A_{\text{S}}} + D. \tag{19}$$

Dividing all the terms of this equation by P,

$$E \approx \frac{|D|}{P}; \qquad \text{rmse} \approx \frac{\text{rms}(D)}{P}. \tag{20}$$

In the planar case, the root mean squared of D, $\text{rms}(D)$, is proportional to $\sqrt{M}$ (Kendall 1948; Huxley 1987, 2003). Extrapolating this fact, we obtain the scaling observed in the Monte Carlo simulation

$$\text{rmse} \propto \frac{\sqrt{M}}{P} \approx \frac{(P/A_{\text{S}})^{1/4}}{P} \propto P^{-3/4}. \tag{21}$$

In the latitude–longitude lattice, the same scaling holds if we consider its smaller sampling efficiency. The latter may be measured with the denominator of (7). This is the number of points of a homogeneous lattice that would do the same work, and is up to ∼36% smaller than P in the range of P considered here. If Fig. 8 is plotted using these effective points in the abscissas, the same fit suffices for both lattice types (Fig. 8, bottom). If the sampling points were placed at random, the rmse would decrease more slowly, as $\propto P^{-1/2}$ (Bevington and Robinson 1992).

7 Conclusions

This paper analyzes the errors involved in measuring the areas of spherical caps using lattices of sampling points: the latitude–longitude lattice (classically used for this task), and a Fibonacci lattice (Swinbank and Purser 2006b). The latter has low anisotropy, is easy to construct, and is shown to result from the intersection of two generative spirals (Fig. 2). A review of the literature (Sect. 3.2) reveals successful applications of this spherical lattice since the 1980s. If the Fibonacci lattice were used instead of its latitude–longitude counterpart, the area measurement would be more efficient, allowing a significant reduction of the computation time. For approximately the same number of lattice points, the maximum root mean squared error would be about 40% smaller (Fig. 8). The maximum errors would be also smaller, and would decay faster with the number of points (Fig. 6). If about a million points were used, as is commonly the case (Feng et al. 2006), the maximum error would be an order of magnitude smaller (Fig. 6).

It is also found that the maximum root mean squared error obeys a single scaling relation when the sampling efficiency is taken into account (Fig. 8). This is partially explained using arguments from similar problems on the plane (Kendall 1948; Huxley 1987, 2003). The area estimate depends also on the orientation of the sampling lattice, especially if the latter has high anisotropy. The difference may be assessed (Hannay and Nye 2004) by rotating the lattice (Greiner 1999). Such an issue is not relevant in the case analyzed here because the caps were placed at random with uniform probability over the spherical surface. Here the Earth's shape has been approximated by a sphere (Kantsiper and Weiss 1998), adding a slightly higher error than other shape models (Kimerling 1984; Earle 2006; Sjöberg 2006). Assessing this difference may be a topic of future research.

Acknowledgements I thank John H. Hannay, Gil Moore, Dimitri Svergun, Richard Swinbank, John Vasquez, Gert Vriend, and Douglas C. Winfield for clarifying different aspects of their work. The results were calculated using the supercomputing facilities of the Institute of Biocomputing and Physics of Complex Systems (BIFI, University of Zaragoza, Spain). Lattice maps were produced with Generic Mapping Tools (Wessel and Smith 1998). I am also grateful to an anonymous reviewer for offering insightful and encouraging comments.

References

Adler I, Barabe D, Jean RV (1997) A history of the study of phyllotaxis. Ann Bot 80(3):231–244

Ahmad R, Deng Y, Vikram DS, Clymer B, Srinivasan P, Zweier JL, Kuppusamy P (2007) Quasi Monte Carlo-based isotropic distribution of gradient directions for improved reconstruction quality of 3D EPR imaging. J Magn Reson 184(2):236–245
Baddeley A, Jensen EBV (2004) Stereology for statisticians. Chapman and Hall–CRC Press, Boca Raton
Barclay M, Galton A (2008) Comparison of region approximation techniques based on Delaunay triangulations and Voronoi diagrams. Comput Environ Urban Syst 32(4):261–267
Bardsley WE (1983) Random error in point counting. Math Geol 15(3):469–475
Bauer R (2000) Distribution of points on a sphere with application to star catalogs. J Guid Control Dyn 23(1):130–137
Bevington PR, Robinson DK (1992) Data reduction and error analysis for the physical sciences, 2nd edn. McGraw Hill, Boston
Bevis M, Cambareri G (1987) Computing the area of a spherical polygon of arbitrary shape. Math Geol 19(4):335–346
Brauchart JS (2004) Invariance principles for energy functionals on spheres. Monatsh Math 141(2):101–117
Bravais L, Bravais A (1837) Essai sur la disposition des feuilles curvisériées. Ann Sci Nat 7:42–110, plates 2–3
Chukkapalli G, Karpik SR, Ethier CR (1999) A scheme for generating unstructured grids on spheres with application to parallel computation. J Comput Phys 149(1):114–127
Conway JH, Sloane NJA (1998) Sphere packings, lattices and groups, 3rd edn. Springer, New York
Cui J, Freeden W (1997) Equidistribution on the sphere. SIAM J Sci Comput 18(2):595–609
Damelin SB, Grabner PJ (2003) Energy functionals, numerical integration and asymptotic equidistribution on the sphere. J Complex 19(3):231–246 [Corrigendum 20(6):883–884]
Dixon R (1987) Mathographics. Basil Blackwell, Oxford
Dixon R (1989) Spiral phyllotaxis. Comput Math Appl 17(4–6):535–538
Dixon R (1992) Green spirals. In: Hargittai I, Pickover CA (eds) Spiral symmetry. World Scientific, Singapore, pp 353–368
Douady S, Couder Y (1992) Phyllotaxis as a physical self-organized growth process. Phys Rev Lett 68(13):2098–2101
Earle MA (2006) Sphere to spheroid comparisons. J Navig 59(3):491–496
Erikson RO (1973) Tubular packing of spheres in biological fine structure. Science 181(4101):705–716
Evans DG, Jones SM (1987) Detecting Voronoi (area-of-influence) polygons. Math Geol 19(6):523–537
Feng S, Ochieng WY, Mautz R (2006) An area computation based method for RAIM holes assessment. J Glob Position Syst 5(1–2):11–16
Fowler DR, Prusinkiewicz P, Battjes J (1992) A collision-based model of spiral phyllotaxis. ACM SIGGRAPH Comput Graph 26(2):361–368
González Á (2009) Self-sharpening seismicity maps for forecasting earthquake locations. Abstracts of the sixth international workshop on statistical seismology. Tahoe City, California, 16–19 April 2009. http://www.scec.org/statsei6/posters.html
Gregory MJ, Kimerling AJ, White D, Sahr K (2008) A comparison of intercell metrics on discrete global grid systems. Comput Environ Urban Syst 32(3):188–203
Greiner B (1999) Euler rotations in plate-tectonic reconstructions. Comput Geosci 25(3):209–216
Gundersen HJG, Jensen EBV, Kiêu K, Nielsen J (1999) The efficiency of systematic sampling in stereology—reconsidered. J Microsc 193(3):199–211
Hannay JH, Nye JF (2004) Fibonacci numerical integration on a sphere. J Phys A 37(48):11591–11601
Howarth RJ (1998) Improved estimators of uncertainty in proportions, point-counting, and pass-fail test results. Am J Sci 298(7):594–607
Hüttig C, Stemmer K (2008) The spiral grid: A new approach to discretize the sphere and its application to mantle convection. Geochem Geophys Geosyst 9(2):Q02018
Huxley MN (1987) The area within a curve. Proc Indian Acad Sci, Math Sci 97(1–3):111–116
Huxley MN (2003) Exponential sums and lattice points III. Proc Lond Math Soc 87(3):591–609
Jarái A, Kozák M, Rózsa P (1997) Comparison of the methods of rock-microscopic grain-size determination and quantitative analysis. Math Geol 29(8):977–991
Jean RV (1994) Phyllotaxis: a systemic study of plant pattern morphogenesis. Cambridge University Press, Cambridge
Kafka AL (2007) Does seismicity delineate zones where future large earthquakes are likely to occur in intraplate environments? In: Stein S, Mazzotti S (eds) Continental intraplate earthquakes: science, hazard, and policy issues. Geological Society of America special paper 425, Boulder, Colorado, pp 35–48

Kantsiper B, Weiss S (1998) An analytic approach to calculating Earth coverage. Adv Astronaut Sci 97:313–332
Kendall DG (1948) On the number of lattice points inside a random oval. Quart J Math Oxford 19(1):1–26
Kimerling AJ (1984) Area computation from geodetic coordinates on the spheroid. Surv Mapp 44(4):343–351
Klíma K, Pick M, Pros Z (1981) On the problem of equal area block on a sphere. Stud Geophys Geod (Praha) 25(1):24–35
Knuth DE (1997) Art of computer programming, 3rd edn. Fundamental algorithms, vol 1. Addison-Wesley, Reading
Kossobokov V, Shebalin P (2003) Earthquake prediction. In: Keilis-Borok VI, Soloviev AA (eds) Nonlinear dynamics of the lithosphere and earthquake prediction. Springer, Berlin, pp 141–207. [References in pp 311–332]
Kozin MB, Volkov VV, Svergun DI (1997) *ASSA*, a program for three-dimensional rendering in solution scattering from biopolymers. J Appl Cryst 30(5):811–815
Kuhlemeier C (2007) Phyllotaxis. Trends Plant Sci 12(4):143–150
Lean JL, Picone JM, Emmert JT, Moore G (2006) Thermospheric densities derived from spacecraft orbits: application to the Starshine satellites. J Geophys Res 111(4):A04301
Li C, Zhang X, Cao Z (2005) Triangular and Fibonacci number patterns driven by stress on core/shell microstructures. Science 309(5736):909–911
Maciá E (2006) The role of aperiodic order in science and technology. Rep Prog Phys 69(2):397–441
Maley PD, Moore RG, King DJ (2002) Starshine: A student-tracked atmospheric research satellite. Acta Astronaut 51(10):715–721
Michalakes JG, Purser RJ, Swinbank R (1999) Data structure and parallel decomposition considerations on a Fibonacci grid. In: Preprints of the 13th conference on numerical weather prediction, Denver, 13–17 September 1999. American Meteorological Society, pp 129–130
Na HS, Lee CN, Cheong O (2002) Voronoi diagrams on the sphere. Comput Geom Theory Appl 23(2):183–194
Niederreiter H (1992) Random number generation and quasi-Monte Carlo methods. Society for Industrial and Applied Mathematics, Philadelphia
Niederreiter H, Sloan IH (1994) Integration of nonperiodic functions of two variables by Fibonacci lattice rules. J Comput Appl Math 51(1):57–70
Nye JF (2003) A simple method of spherical near-field scanning to measure the far fields of antennas or passive scatterers. IEEE Trans Antenna Propag 51(8):2091–2098
Ochieng WY, Sheridan KF, Sauer K, Han X (2002) An assessment of the RAIM performance of a combined Galileo/GPS navigation system using the marginally detectable errors (MDE) algorithm. GPS Solut 5(3):42–51
Prusinkiewicz P, Lindenmayer A (1990) The algorithmic beauty of plants. Springer, New York
Purser RJ (2008) Generalized Fibonacci grids: A new class of structured, smoothly adaptive multi-dimensional computational lattices. Office Note 455, National Centers for Environmental Prediction, Camp Springs, MD, USA
Purser RJ, Swinbank R (2006) Generalized Euler-Maclaurin formulae and end corrections for accurate quadrature on Fibonacci grids. Office Note 448, National Centers for Environmental Prediction, Camp Springs, MD, USA
Rakhmanov EA, Saff EB, Zhou YM (1994) Minimal discrete energy on the sphere. Math Res Lett 1(6):647–662
Ridley JN (1982) Packing efficiency in sunflower heads. Math Biosci 58(1):129–139
Ridley JN (1986) Ideal phyllotaxis on general surfaces of revolution. Math Biosci 79(1):1–24
Saff EB, Kuijlaars ABJ (1997) Distributing many points on a sphere. Math Intell 19(1):5–11
Sigler LE (2002) Fibonacci's Liber Abaci: a translation into modern English of Leonardo Pisano's book of calculation. Springer, New York
Singh P (1985) The so-called Fibonacci numbers in ancient and medieval India. Hist Math 12(3):229–244
Sjöberg LE (2006) Determination of areas on the plane, sphere and ellipsoid. Surv Rev 38(301):583–593
Sloan IH, Joe S (1994) Lattice methods for multiple integration. Oxford University Press, London
Svergun DI (1994) Solution scattering from biopolymers: advanced contrast-variation data analysis. Acta Cryst A 50(3):391–402
Swinbank R, Purser RJ (1999) Fibonacci grids. In: Preprints of the 13th conference on numerical weather prediction, Denver, 13–17 September 1999. American Meteorological Society, pp 125–128
Swinbank R, Purser RJ (2006a) Standard test results for a shallow water equation model on the Fibonacci grid. Forecasting Research Technical Report 480, Met Office, Exeter, UK

Swinbank R, Purser RJ (2006b) Fibonacci grids: a novel approach to global modelling. Q J R Meteorol Soc 132(619):1769–1793
Van den Dool HM (2007) Empirical methods in short-term climate prediction. Oxford University Press, London
Vogel H (1979) A better way to construct the sunflower head. Math Biosci 44(3–4):179–189
Vriend G (1990) WHAT IF: a molecular modeling and drug design program. J Mol Graph 8(1):52–56
Weiller AR (1966) Probleme de l'implantation d'une grille sur une sphere, deuxième partie. Bull Géod 80(1):99–111
Weisstein EW (2002) CRC concise encyclopedia of mathematics CD-ROM, 2nd edn. CRC Press, Boca Raton
Wessel P, Smith WHF (1998) New, improved version of Generic Mapping Tools released. Eos Trans Am Geophys Union 79(47):579
Williamson DL (2007) The evolution of dynamical cores for global atmospheric models. J Meteorol Soc Jpn B 85:241–269
Winfield DC, Harris KM (2001) Phyllotaxis-based dimple patterns. Patent number WO 01/26749 Al. World Intellectual Property Organization
Zaremba SK (1966) Good lattice points, discrepancy, and numerical integration. Ann Mat Pura Appl 73(1):293–317